Title

ON THE INFLUENCE OF FATIGUE UNDERLOADS ON CYCLIC CRACK GROWTH AT LOW STRESS INTENSITIES

Authors

Suresh, S.
Ritchie, R.O.

Publication Date

1981-05-01

LBL-13353
Preprint

Lawrence Berkeley Laboratory
UNIVERSITY OF CALIFORNIA

Materials & Molecular Research Division

Submitted to Materials Science and Engineering

ON THE INFLUENCE OF FATIGUE UNDERLOADS ON CYCLIC CRACK GROWTH AT LOW STRESS INTENSITIES

S. Suresh and R.O. Ritchie

May 1981

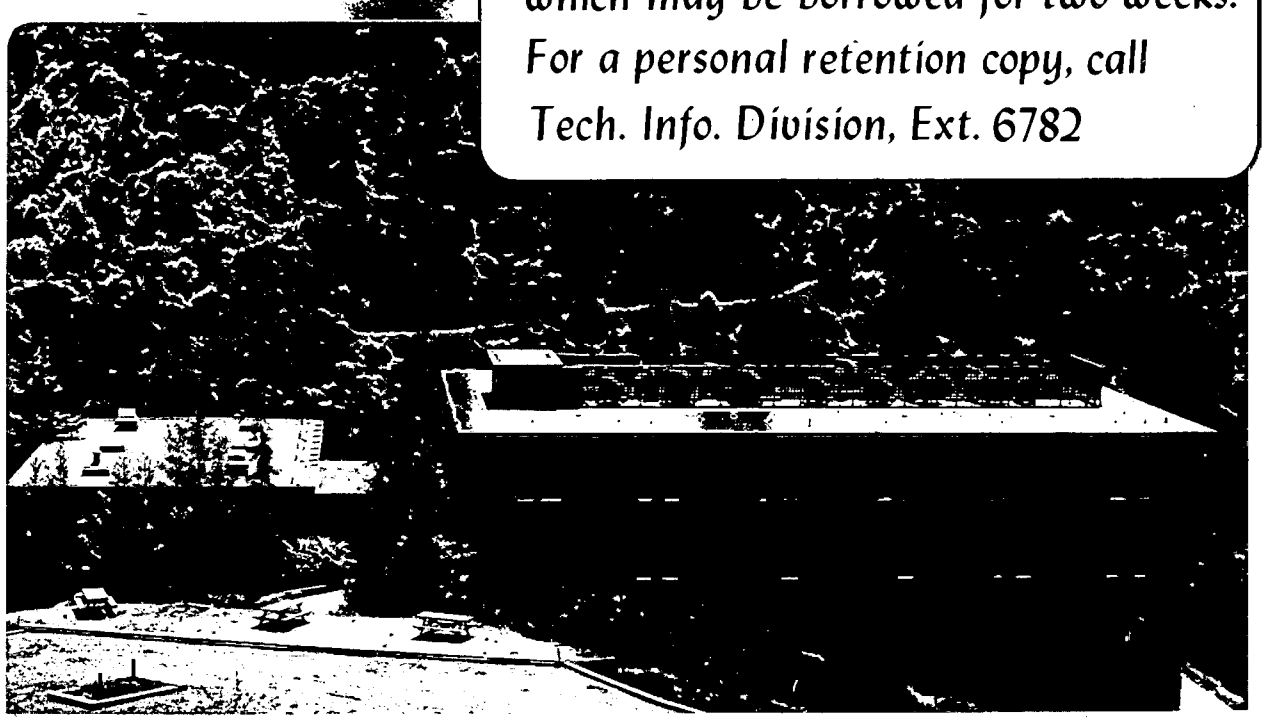

Prepared for the U.S. Department of Energy under Contract W-7405-ENG-48

DISCLAIMER

ON THE INFLUENCE OF FATIGUE UNDERLOADS ON CYCLIC CRACK GROWTH AT LOW STRESS INTENSITIES

S. Suresh* and R. O. Ritchie*
Materials and Molecular Research Division of the Lawrence Berkeley Laboratory, and the Department of Materials Science and Mineral Engineering, University of California, Berkeley, California 94720.

Summary

The influence of variable amplitude loading in the form of block underload cycling is examined for(plane strain) near-threshold fatigue crack propagation in a bainitic 2¼Cr-1Mo pressure vessel steel (ASTM A542 Class 3), tested in ambient temperature moist air at low load ratios (R=0.05). It is shown that the application of fatigue underloads with stress intensity ranges *below* the threshold (ΔK_o) can result in significant transient retardations in initial growth rates when cycling is subsequently resumed at baseline levels above the threshold. The magnitudes of the retardations are found to be dependent upon baseline (ΔK_B) and underload (ΔK_u) stress intensities. Using ESCA and scanning Auger spectroscopy, the observations are shown to be consistent with concepts of oxide-induced crack closure, which arises from extra corrosion debris (Fe_2O_3) generated within the near-threshold crack during the underload cycling period. Such oxide deposits, being of the order of pulsating crack tip displacements (ΔCTOD) can lead to increased closure loads and reduced effective stress intensity ranges, thereby retarding subsequent initial growth rates at baseline levels. It is shown that sub-threshold fatigue underloads have negligible effects on baseline near-threshold growth rates

---

* Formerly with the Department of Mechanical Engineering, Massachusetts Institute of Technology, Cambridge, Ma. 02139.

when the underload ΔCTOD appears smaller than the existing (baseline) excess oxide thickness. In this instance, the crack remains effectively closed during underload cycling, thus restricting further oxide growth. The relevance of these observations to current procedures for the determination of threshold values and slow crack growth rates at low stress intensities is discussed in detail.

Nomenclature

a	crack length
a^*	crack length over which retardation occurs (Fig. 1)
d	excess oxide thickness measured on fracture surfaces
da/dN	fatigue crack growth rate per cycle
$(da/dN)_B$	baseline fatigue crack growth rate at ΔK_B (Fig. 1)
$(da/dN)_S$	initial fatigue crack growth rate following underload (Fig. 1)
E	elastic modulus
K_I	linear elastic stress intensity factor (Mode I)
K_{Ic}	plane strain fracture toughness
K_{max}	maximum stress intensity during fatigue cycle
K_{min}	minimum stress intensity during fatigue cycle
N	number of cycles
N^*	number of cycles over which retardation occurs (Fig. 1)
n'	work hardening exponent (cyclic)
R	load ratio (K_{min}/K_{max})
$\Delta CTOD$	pulsating crack tip opening displacement
ΔK	alternating stress intensity ($K_{max} - K_{min}$)
ΔK_B	baseline alternating stress intensity (Fig. 1)
ΔK_o	threshold stress intensity for crack growth
ΔK_u	alternating stress intensity at underload (Fig. 1)
ΔK_{uc}	critical value of underload stress intensity
σ_y'	cyclic yield strength

1. INTRODUCTION

In recent years, considerable effort has been directed towards understanding the role of variable amplitude loading on fatigue crack propagation in engineering materials (e.g. 1-8). In particular, transients in growth rate behavior induced by single tensile overloads or various spectrum loading sequences have been attributed to such mechanisms as residual compressive stresses (1,2), cyclic strain hardening (6), crack tip blunting (7), and plasticity-induced crack closure (8). Since such phenomena are important for airframe components, many of these studies have been performed with thin sheets (1-5) under essentially plane stress conditions, where mechanisms such as plasticity-induced crack closure can be predominant (8).

In this study, however, we examine the role of variable amplitude loading under fully plane strain conditions, and specifically consider the influence of block cycling *below* the so-called threshold stress intensity for no crack growth (ΔK_o). Such underloads may occur within certain service loading spectra, and during laboratory testing using standard load-shedding procedures (9,10) for measuring near-threshold growth rates at low stress intensities. For example, since measurement of such near-threshold crack growth at conventional frequencies can be very time-consuming, it is often necessary to interrupt the test, by say "stopping" or "parking" overnight at a ΔK level below the threshold ΔK_o where presumably no damage can occur. Where such interruptions have been reported, unexplained transients in crack growth behavior often result, where behavior after the interruption is initially very different

from behavior before, for nominally identical conditions. (11). In the present work, the influence of periodic cycling at ΔK levels below the threshold ΔK_o is examined on near-threshold fatigue crack propagation in a bainitic 2¼Cr-1Mo pressure vessel steel. The transient growth rate behavior observed is rationalized in terms of a new mechanism of microscopic crack closure (12-14) involving the role of enlarged crack tip oxide deposits in generating increased closure loads.

2. EXPERIMENTAL PROCEDURES

Studies were performed on a 175 mm thick plate of 2¼Cr-1Mo pressure vessel steel, received in the water quenched and 663°C tempered condition. The steel, ASTM A542 Class 3, hereafter referred to as SA542-3, of composition given below

C	Mn	Si	Ni	Cr	Mo	P	S	Cu
0.12	0.45	0.21	0.11	2.28	1.05	0.014	0.015	0.12

was found to be fully bainitic (<3% free ferrite) uniformly throughout the thickness. Ambient temperature mechanical properties are listed in Table 1.

Fatigue crack propagation experiments were conducted with 12.7 mm thick compact specimens, machined in the T-L orientation between quarter and mid-thickness. Based on the criterion that maximum plastic zone sizes were always less than 1/15 of test-piece thickness, all tests in this study were conducted under fully plane strain conditions. Testing was performed on 50 kN Instron electro servo-hydraulic testing machines

operating under load control at 50 Hz (sine wave) at a constant load ratio (R = ratio of minimum to maximum load) of 0.05. Cracks were grown in ambient temperature moist air (30 pct relative humidity), and were continuously monitored using D.C. electrical potential techniques (e.g. 15). Full experimental details are described elsewhere (9,12,14,15).

Near-threshold growth rates (for constant amplitude cycling) were determined by a load-shedding procedure. Growth rates were monitored over crack length increments representing at least four times the previous *maximum* plastic zone size, before loads were reduced by not more than 10%, and the same procedure repeated. The threshold ΔK_o, representing the alternating stress intensity below which cracks are dormant or grow at experimentally undetectable rates, was operationally defined in terms of a maximum growth rate of 10^{-8} mm/cycle (9).

The influence of variable amplitude loading was examined at a constant load ratio (R = 0.05) using loading sequences illustrated in Fig. 1. After load-shedding to near-threshold levels, cracks were grown for 1 mm at a constant baseline ΔK level (ΔK_B), whereupon a sub-threshold fatigue underload (ΔK_u) was applied for 2.7×10^6 cycles (15 hrs at 50 Hz), before conditions were returned to the original ΔK_B baseline level. A series of tests was performed, for baseline levels of ΔK_B = 8.3 - 10 MPa$\sqrt{m}$, with underloads (below ΔK_o) of ΔK_u = 4 - 7.5 MPa$\sqrt{m}$. From crack length (a) versus number of cycles (N) data monitored during the sequence, the following parameters were defined (Fig. 1); namely $(da/dN)_B$, the baseline crack growth rate at ΔK_B; $(da/dN)_S$, the initial crack growth rate at ΔK_B following the underload period; and a^* and N^*, representing the crack length and number of cycles at ΔK_B following the underload period

before growth rates return to their original baseline value $(da/dN)_B$.

Fracture surfaces were examined using scanning electron microscopy and the extent of surface corrosion deposits assessed with Ar^+ sputtering techniques using Auger spectroscopy. Procedures for analyzing oxide composition and estimating oxide thicknesses formed within near-threshold cracks tested are described in details elsewhere (14).

3. RESULTS

Constant amplitude fatigue crack propagation behavior for SA542-3 steel, spanning a wide range of growth rates from 10^{-8} to 10^{-3} mm/cycle, is shown in Fig. 2 for tests in moist air at $R = 0.05$ and 0.75. A threshold for crack growth of $\Delta K_o = 7.7$ MPa$\sqrt{m}$ is apparent for behavior at $R = 0.05$. Fractography associated with such data indicated a predominately transgranular fracture at near-threshold stress intensities, with evidence of isolated intergranular facets (Fig. 3).

Effects of sub-threshold underloads ($\Delta K_u < \Delta K_o$) on near-threshold crack growth rates at baseline ΔK_B levels between 8.3 and 10 MPa$\sqrt{m}$ ($R = 0.05$) are shown in Fig. 4. Data pertinent to this figure, in terms of parameters defined in Fig. 1, are listed in Table 2. Although no crack growth was ever detected during the 2.7×10^6 underload cycles, subsequent crack growth was in certain cases severely affected. Little effect was apparent after a fatigue underload of $\Delta K_u = 4$ MPa$\sqrt{m}$ on baseline growth rates at $\Delta K_B = 10$ MPa$\sqrt{m}$ (Fig. 4a). Similarly, underload cycling at $\Delta K_u = 6.5$ MPa$\sqrt{m}$ had only a small influence on crack growth at $\Delta K_B = 9$ MPa$\sqrt{m}$ (Fig. 4b). Underload cycling fractionally below the

threshold at ΔK_u = 7.5 MPa$\sqrt{m}$, however, resulted in significant decelerations in subsequent baseline growth rates at ΔK_B between 8.3 and 10 MPa$\sqrt{m}$ (Fig. 4 c-f). Following the underload periods, initial growth rates were up to 5 times slower than pre-underload baseline rates, with retardations experienced over subsequent crack lengths (a^*) of up to 0.3 mm (equivalent to several times maximum plastic zone sizes at ΔK_B) .

Thus, periods of fatigue underload cycles beneath the threshold ΔK_o , where presumably no crack growth damage can occur, can give rise to significant transient retardations in near-threshold crack growth rates over distances comparable with several maximum plastic zone sizes, the magnitude of the retardation depending both on the baseline and underload stress intensities applied.

4. DISCUSSION

It has been shown that, in certain circumstances, cycling *below the threshold stress intensity* ΔK_o can retard subsequent near-threshold crack growth rates, a phenomenon somewhat analogous to the well-known effect of "coaxing" where smooth specimens cycled *below the fatigue limit* are often found to possess improved resistance to fatigue failure. However, whereas coaxing has been attributed to strain-ageing effects (16), a mechanism for the influence of sub-threshold underloads is presented below in terms of crack closure arguments, involving the role of crack tip corrosion debris in increasing closure loads.

It has been reported by several workers (e.g. 9,12-14,17) that,

particularly in steels, near-threshold fatigue crack propagation in moist environments is accompanied by excess oxide formation within the crack. Such deposits, which predominate only at lower load ratios (Fig. 5), can be as much as twenty times thicker than the background oxide thickness (i.e. naturally-formed oxide on freshly-bared metal exposed to the same environment for the same time period) as growth rates approach the threshold. "Fretting oxidation" has been suggested as a mechanism for the enlarged oxide production, whereby continual breaking and compacting of the oxide scale takes place behind the crack tip due to abrasion between fracture surfaces (12,14,17). This abrasion itself occurs only at low load ratios, typically below $R = 0.5$, and can be attributed to plasticity-induced crack closure (18) and larger Mode II crack tip displacements (19) which are characteristic of crack growth at very low stress intensities (14). At near-threshold levels, the corrosion debris is of comparable size to the pulsating crack tip displacements (ΔCTOD), and thus a microscopic form of crack closure can occur in the presence of the oxide as a result of earlier contact between the fracture surfaces during the decreasing portion of the loading cycle (12-14). This leads to higher closure loads, and lower effective stress intensity ranges at crack tip, i.e. the presence of the excess oxide debris effectively raises K_{min}, a fact that has recently been demonstrated experimentally using ultrasonic techniques (20). Since the nature of the environment and the extent of plasticity-induced crack closure can govern the extent of excess oxide formation, this mechanism termed "oxide-induced crack closure" has proved to be very effective in rationalizing effects of load ratio (12) and environment (12,14) on near-threshold fatigue

crack growth observed in lower strength steels at both ambient (12-14,20) and elevated (21) temperatures.

For the present crack growth results (Fig. 2), Ar^+ sputtering analysis of fracture surfaces in the Auger spectrometer revealed actual oxide thicknesses as large as 0.2 μm , as shown in Fig. 6 as a function of crack length and crack growth rate. The thickness (d) of the oxide (identified with ESCA to be Fe_2O_3) is seen to vary inversely with growth rate, and to be at a maximum near ΔK_o (at R = 0.05). At high load ratios (R = 0.75), thicknesses are much smaller (~50-150 Å), and are of the order of the naturally-formed background oxide thickness. Since one unit volume of Fe produces 2.13 unit volumes of Fe_2O_3 , the oxide thickness measurements shown in Fig. 6 represent approximately the total excess material inside the crack, assuming equal deposits on each crack face. Recent studies in 2¼Cr-1Mo steels, tested in air, water, helium and hydrogen environments, show that at threshold, the maximum excess oxide thickness is comparable in size with the pulsating crack tip opening displacement (Fig. 7), which perhaps provides one plausible reason for the existence of a threshold since at ΔK_o the crack will be effectively wedged-closed (14).

Using such concepts of oxide-induced crack closure, the observed effects of sub-threshold underload cycling can readily be explained. First, we conclude from the data shown in Figs. 6 and 7 that i) oxide thicknesses increase with decreasing growth rates and hence with decreasing ΔK levels as the threshold is approached, and ii) cracks will not propagate when the maximum excess oxide thickness equals the pulsating crack tip opening displacement (ΔCTOD). Thus, for particular com-

binations of baseline ΔK_B and underload ΔK_u, it follows that if the excess oxide thickness d formed at baseline ΔK_B is less than the ΔCTOD at underload ΔK_u, then the application of sub-threshold underload cycles, while not generating fatigue damage *per se*, can result in further oxide formation due to fretting oxidation mechanisms. Thus, on returning to the baseline ΔK_B level following the underload cycling, one might expect in this instance some initial retardation in crack growth rates due to the increased crack closure loads from the extra oxide deposits formed at ΔK_u. If, on the other hand, the excess oxide thickness d at ΔK_B is already larger than the underload ΔCTOD, then little effect of the underload cycling would be expected, since during the latter period, the crack would be effectively wedged-closed, thereby limiting further oxidation.

This concept is illustrated in Fig. 8, where the variation of crack growth rates (da/dN), experimentally measured oxide thickness (d) and computed underload pulsating crack tip displacements $(\Delta CTOD)^*$ are all plotted as a function of ΔK. Considering first the situation of a baseline ΔK_B of 10 MPa$\sqrt{m}$, the oxide thickness generated at this level has been measured to be approximately 0.11 μm (Fig. 8). When an underload of ΔK_u = 4 MPa$\sqrt{m}$ is applied, the corresponding ΔCTOD is roughly 0.05 μm, smaller than the existing oxide thickness, such that the crack effectively remains closed. With no enhancement in oxide-induced crack closure, therefore, an underload of 4 MPa$\sqrt{m}$ would be expected to have little effect on growth rates at 10 MPa$\sqrt{m}$, in accordance

*Pulsating crack displacement is defined from $\Delta CTOD = 0.5\ \Delta K_u^2 / 2\sigma_y' E$, where E is the elastic modulus, and σ_y' the cyclic yield strength (22). Computations are for a material in plane strain with work hardening exponent (n') of 0.15, and yield strain (σ_y'/E) of 0.002.

with experimental observations (Fig. 4a and Table 2). Conversely, when an underload of $\Delta K_u = 7.5$ MPa$\sqrt{m}$ is applied at $\Delta K_B = 10$ MPa$\sqrt{m}$, the underload ΔCTOD is now $\sim$0.17 μm, larger than the existing (baseline) oxide thickness, such that some further oxide growth can occur (even though no crack growth takes place). With the resulting enhancement in oxide-induced crack closure, the 7.5 MPa$\sqrt{m}$ underload would be expected to cause some initial retardation in growth rates at $\Delta K_B = 10$ MPa$\sqrt{m}$, consistent with experimental results (Fig. 4f and Table 2). Similar arguments are applicable to the other results in Fig. 4.

It also follows from this discussion that at each baseline ΔK_B level, a critical underload stress intensity range (ΔK_{uc}) will exist below which underloads can have little effect on subsequent crack growth rates. This corresponds to an underload ΔK_u level below which the crack remains closed, i.e. where the underload ΔCTOD is less than the existing oxide thickness (d). For crack growth at $\Delta K_B = 10$ MPa$\sqrt{m}$ (where $d \approx 0.11$ μm), this corresponds to an underload level of $\Delta K_{uc} = 6$ MPa$\sqrt{m}$. Hence, underloads at 7.5 MPa$\sqrt{m}$ can lead to subsequent retardations whereas underloads at 4 MPa$\sqrt{m}$ have little effect (Table 2). Similarly, for crack growth at $\Delta K_B = 9$ MPa$\sqrt{m}$, where critical underload levels become $\Delta K_{uc} = 7.1$ MPa$\sqrt{m}$, underloads at 7.5 MPa$\sqrt{m}$ are seen to reduce growth rates initially by roughly five times, whereas negligible effects are apparent following underloads at 6.5 MPa$\sqrt{m}$ (Fig. 4b and d). Using Fig. 8, values of ΔK_{uc} can be simply estimated graphically for any baseline ΔK_B level, by following the direction of the arrows in equating oxide thickness (d) at ΔK_B to ΔCTOD at ΔK_u. However, recognizing that oxide-induced crack closure is only important at low stress intensities

where crack tip displacements and corrosion deposits are of the same size-scale, it is apparent that sub-threshold underloads are only likely to have an effect on near-threshold growth rates. With increasing ΔK levels, the corresponding $\Delta CTOD$ increases so rapidly (proportional to ΔK^2) that further oxidation during the underload would be negligible in comparison.

Thus, in summary, it has been shown that near-threshold fatigue crack growth can suffer transient retardations following underload cycling (at the same load ratio) below the threshold. Such crack growth retardations are reasoned to result from enhanced oxide-induced crack closure generated during the underload, provided that the underload $\Delta CTOD$ is large enough to allow further oxide growth. The close numerical correspondence between $\Delta CTOD$ and crack flank oxide thickness data, however, could be considered as somewhat fortuitous in view of the uncertainty in the two measurements, but conceptually such data are totally consistent with an explanation of the experimental observations in terms of oxide-induced crack closure.

In terms of recommended procedures for measuring near-threshold fatigue crack growth and threshold ΔK_o values (10), such closure concepts could have important consequences. Current practices for threshold determination utilize crack growth monitoring under decreasing ΔK (load-shedding) and/or increasing ΔK conditions, thus continuously involving variable-amplitude loading. Care is generally taken to avoid too rapid a descent in ΔK to minimize crack growth retardation and hence premature threshold determination resulting from plasticity considerations. It is now apparent that a further factor may be important in that in-

terrupting tests, say by "parking" overnight at ΔK levels below the threshold, may yield similar premature retardations. Further, where oxide-induced closure is significant, one might expect that near-threshold growth rates determined under decreasing ΔK conditions may be somewhat different from those determined under increasing ΔK. In this regard, it is perhaps significant that materials which are very susceptible to aqueous stress corrosion cracking are often most likely to show this behavior (10,23), possibly reflecting a differing contribution from oxide-induced closure arising from the presence of substantial crack flank corrosion deposits.

5. CONCLUSIONS

Based on a study in plane strain of variable amplitude loading on near-threshold fatigue crack propagation in a bainitic 2¼Cr-1Mo pressure vessel steel, tested at low load ratios ($R = 0.05$) in moist ambient temperature air, the following conclusions are drawn:

1) Despite the complexities associated with experimental measurements, the threshold for fatigue crack growth (ΔK_o) is consistent with pulsating crack tip displacements of the order of the maximum excess oxide thickness.

2) Block underload cycles (2.7×10^6 cycles per block) at alternating stress intensities *below* the threshold (ΔK_o) can result in significant transient retardations in initial growth rates when cycling in subsequently resumed at baseline levels, the magnitude of the effect being critically dependent upon underload (ΔK_u) and baseline (ΔK_B) stress intensities.

3) The transient growth rate behavior appears to be consistent with concepts of oxide-induced crack closure, where extra corrosion debris is generated within the crack during underload cycling, resulting in higher closure loads, lower effective stress intensity ranges and hence retarded initial growth rates at subsequent baseline levels.

4) The lack of such crack growth retardation effects for certain combinations of underload (ΔK_u) and baseline (ΔK_B) levels is found to occur when pulsating crack tip displacements (ΔCTOD) at the underload are smaller than the existing excess oxide thickness. Here it is reasoned that since the crack remains effectively closed during underload cycling, further oxide growth would be restricted.

ACKNOWLEDGEMENT

This work was supported by the Director, Office of Energy Research, Office of Basic Energy Sciences, Materials Sciences Division of the U. S. Department of Energy under Contract Number W-7405-ENG-48.

REFERENCES

1) H. F. Hardrath and A. J. McEvily, Proc. Crack Prop. Symp. 1, Cranfield, England, 1961.

2) J. Schijve and D. Broek, Aircr. Eng. 34 (1962) 314.

3) E.F.J. von Euw, R. W. Hertzberg, and R. Roberts, ASTM STP 513, 1972, p. 230.

4) J. Willensborg, R. M. Engle and H. A. Wood, Tech. Mem. 71-1-FBR, 1971.

5) D. E. Wheeler, J.Basic Eng.,(Trans. ASME Ser.D),94 (1972) 181.

6) R. E. Jones, Eng. Fract. Mech., 5 (1973) 585.

7) J. R. Rice, ASTM STP 415, 1967, p. 247.

8) W. Elber, ASTM STP 559, 1974, p. 45.

9) R. O. Ritchie, Intl. Metals Reviews, 20 (1979)205.

10) R. J. Bucci, Proc. ASTM E-9/E-24 Symposium on Fatigue Crack Growth Measurement and Data Analysis, Pittsburgh, PA. Oct. 1979.

11) G. A. Miller, S. J. Hudak, and R. P. Wei, J. Test. Eval., 1 (1973) 524.

12) R. O. Ritchie, S. Suresh and C. M. Moss, J. Eng. Mater. Technol. (Trans. ASME Ser. H), 102 (1980) 293.

13) A. T. Stewart, Eng. Fract. Mech., 13 (1980) 463.

14) S. Suresh, G. F. Zamiski, and R. O. Ritchie, Met. Trans. A., 12A (1981).

15) G. H. Aronson and R. O. Ritchie, J.Test. Eval., 7 (1979) 208.

16) J. F. Knott, Fundamentals of Fracture Mechanics , Butterworths, London, 1973 .

17) D. Benoit, R. Namdar-Tixier and R. Tixier, Mater. Sci. Eng, 45 (1980) 1.

18) W. Elber, Damage Tolerance in Aircraft Structures, ASTM STP 486, 1971, p. 280.

19) D. L. Davidson, Fatigue Eng. Matls. Struc., 3 (1981) 229.

20) S. Suresh, Sc.D. Thesis, Department of Mechanical Engineering, M.I.T., 1981.

21) R. P. Skelton and J. R. Haigh, Mater. Sci. Eng., 36 (1978) 17.

22) C. F. Shih, J. Mech.Phys.Solids, 29 (1981).

23) R. J. Bucci, unpublished work, Alcoa Technical Center, PA, 1980.

Table 1: Ambient Temperature Mechanical Properties of SA542-3

Yield Strength[1]		U.T.S.	Redn. in Area	Elong.[2]	K_{Ic}
monotonic	cyclic[3]				
(MPa)		(MPa)	(%)	(%)	(MPa$\sqrt{m}$)
500	400	610	77	25	295

[1] 0.2% offset yield strengths

[2] 45 mm gauge length

[3] measured using incremental-step tests.

Table 2:

Results[1] of Variable Amplitude Tests involving Effects of Underloads (ΔK_u) on Near-Threshold Growth

Test No.	$\Delta K_B \rightarrow \Delta K_u \rightarrow \Delta K_B$ (MPa$\sqrt{m}$)	$\left(\frac{da}{dN}\right)_B \rightarrow \left(\frac{da}{dN}\right)_S$ (mm/cycle)	a^* (mm)	N^* (cycles)
a	$10 \rightarrow 4 \rightarrow 10$	$3 \times 10^{-6} \rightarrow 3 \times 10^{-6}$	0.010	1.5×10^4
b	$9 \rightarrow 6.5 \rightarrow 9$	$1 \times 10^{-6} \rightarrow 8.5 \times 10^{-7}$	0.008	1.5×10^4
c	$8.3 \rightarrow 7.5 \rightarrow 8.3$	$4 \times 10^{-7} \rightarrow 1.4 \times 10^{-7}$	0.100	8.0×10^5
d	$9 \rightarrow 7.5 \rightarrow 9$	$1 \times 10^{-6} \rightarrow 2 \times 10^{-7}$	0.140	6.5×10^5
e	$9.5 \rightarrow 7.5 \rightarrow 9.5$	$2.5 \times 10^{-6} \rightarrow 6.5 \times 10^{-7}$	0.300	5.0×10^5
f	$10 \rightarrow 7.5 \rightarrow 10$	$3 \times 10^{-6} \rightarrow 1.2 \times 10^{-6}$	0.240	1.5×10^5

[1]Definition of parameters given in text and in Fig. 1

LIST OF FIGURE CAPTIONS

Fig. 1: Schematic illustration of the loading sequence used for constant ΔK_I underload tests. ΔK_B is the baseline stress intensity, ΔK_u the underload stress intensity, and ΔK_o the fatigue crack growth threshold.

Fig. 2: Constant amplitude data showing variation of fatigue crack propagation rates (da/dN) in bainitic SA542-3 steel as a function of ΔK . Tests are for $R = 0.05$ and 0.75 in moist ambient temperature air at a frequency of 50 Hz.

Fig. 3: Fractography of near-threshold fatigue crack growth in SA542-3 tested in moist air at $\Delta K = 8$ MPa$\sqrt{m}$ ($R = 0.05$).

Fig. 4: Crack length (a) versus number of cycles (N) data for underload tests, showing behavior prior to and immediately following the underload.

Fig. 5: Bands of corrosion deposits visible on near-threshold fatigue fracture surfaces tested in moist air at $R = 0.05$ and 0.75.

Fig. 6: Measurement of crack flank oxide thickness (d) as a function of crack length (a) and crack growth rate (da/dN) for SA542-3 tested at $R = 0.05$ and 0.75 in moist air. Data from Ar^+ sputtering analysis using Auger spectroscopy.

Fig. 7: Correspondence of maximum excess oxide thickness with pulsating crack tip displacement (ΔCTOD) at the fatigue crack growth threshold ΔK_o, for a range of 2¼Cr-1Mo steels.

Fig. 8: Crack growth rates (da/dN), measured excess oxide thickness (d), and computed pulsating crack tip displacements (ΔCTOD) as a function of ΔK for near-threshold fatigue behavior in SA542-3, showing potential influence of underload ΔK_u on baseline ΔK_B growth rates.

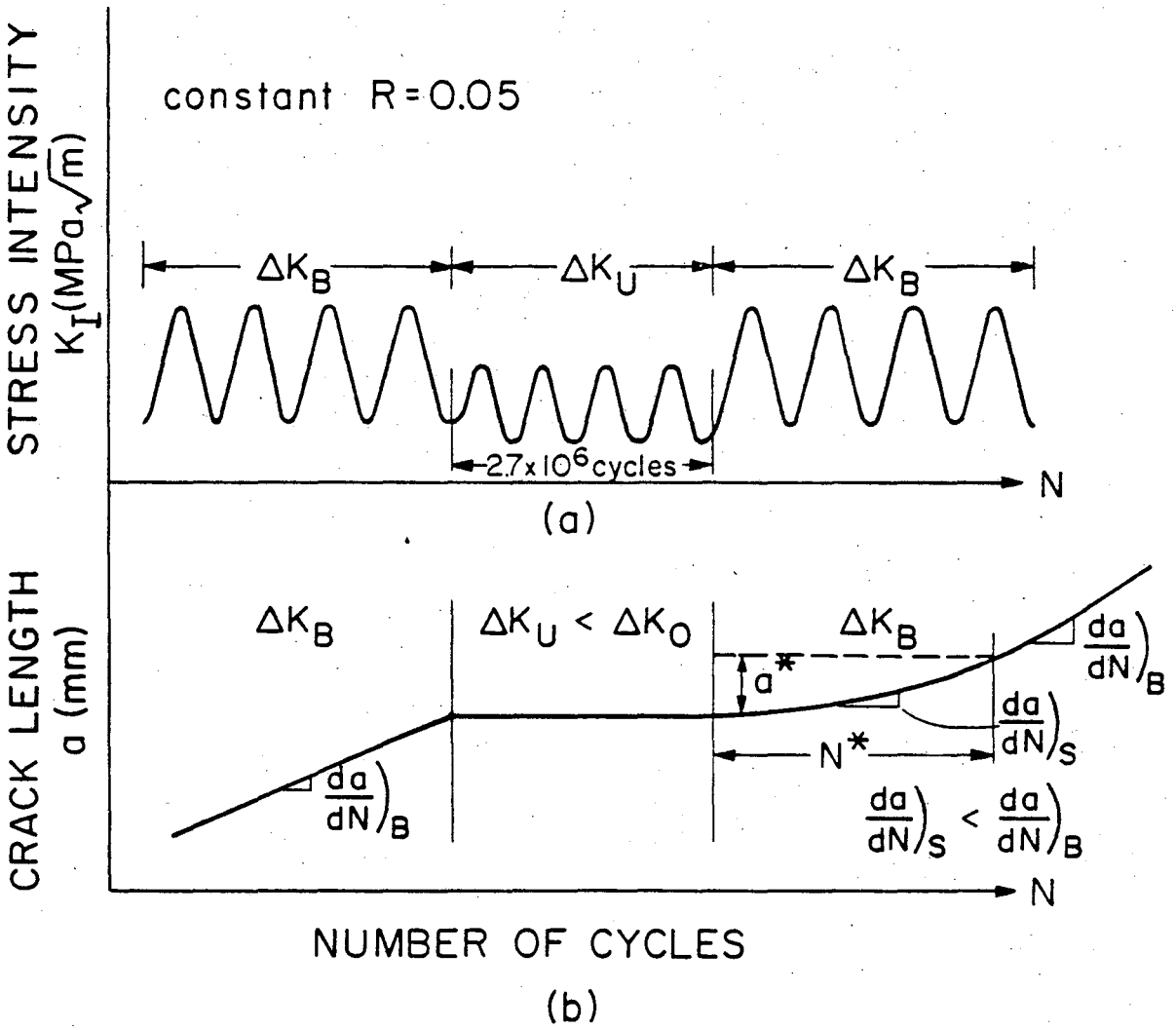

Figure 1

Schematic illustration of the loading sequence used for constant ΔK_I underload tests. ΔK_B is the baseline stress intensity, ΔK_u the underload stress intensity, and ΔK_o the fatigue crack growth threshold.

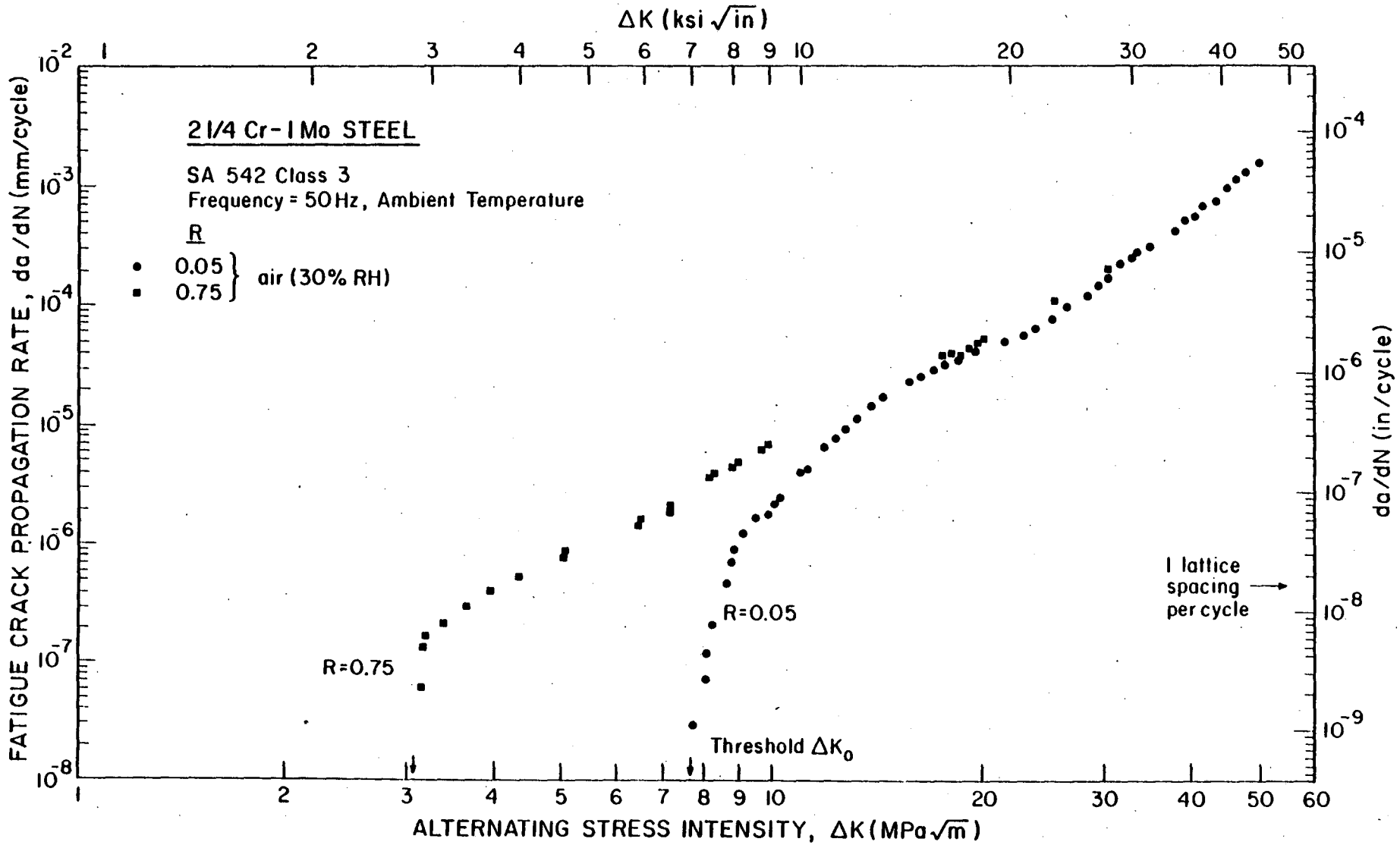

Figure 2

Constant amplitude data showing variation of fatigue crack propagation rates (da/dN) in bainitic SA542-3 steel as a function of ΔK. Tests are for $R = 0.05$ and 0.75 in moist ambient temperature air at a frequency of 50 Hz.

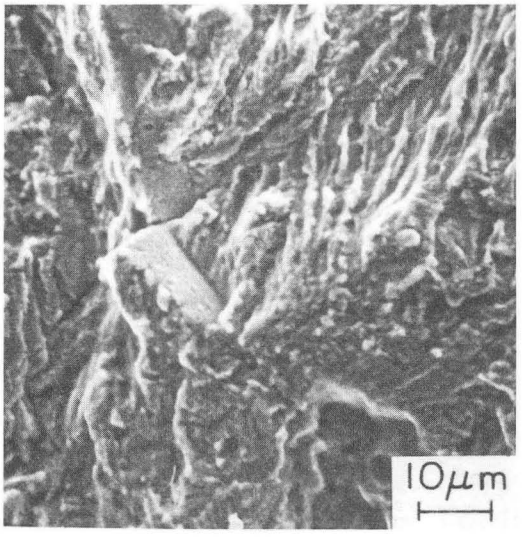

XBB 8110-9787

Figure 3

Fractography of near-threshold fatique crack growth in SA542-3 tested in moist air at $\Delta K = 8$ MPa$\sqrt{m}$ ($R = 0.05$).

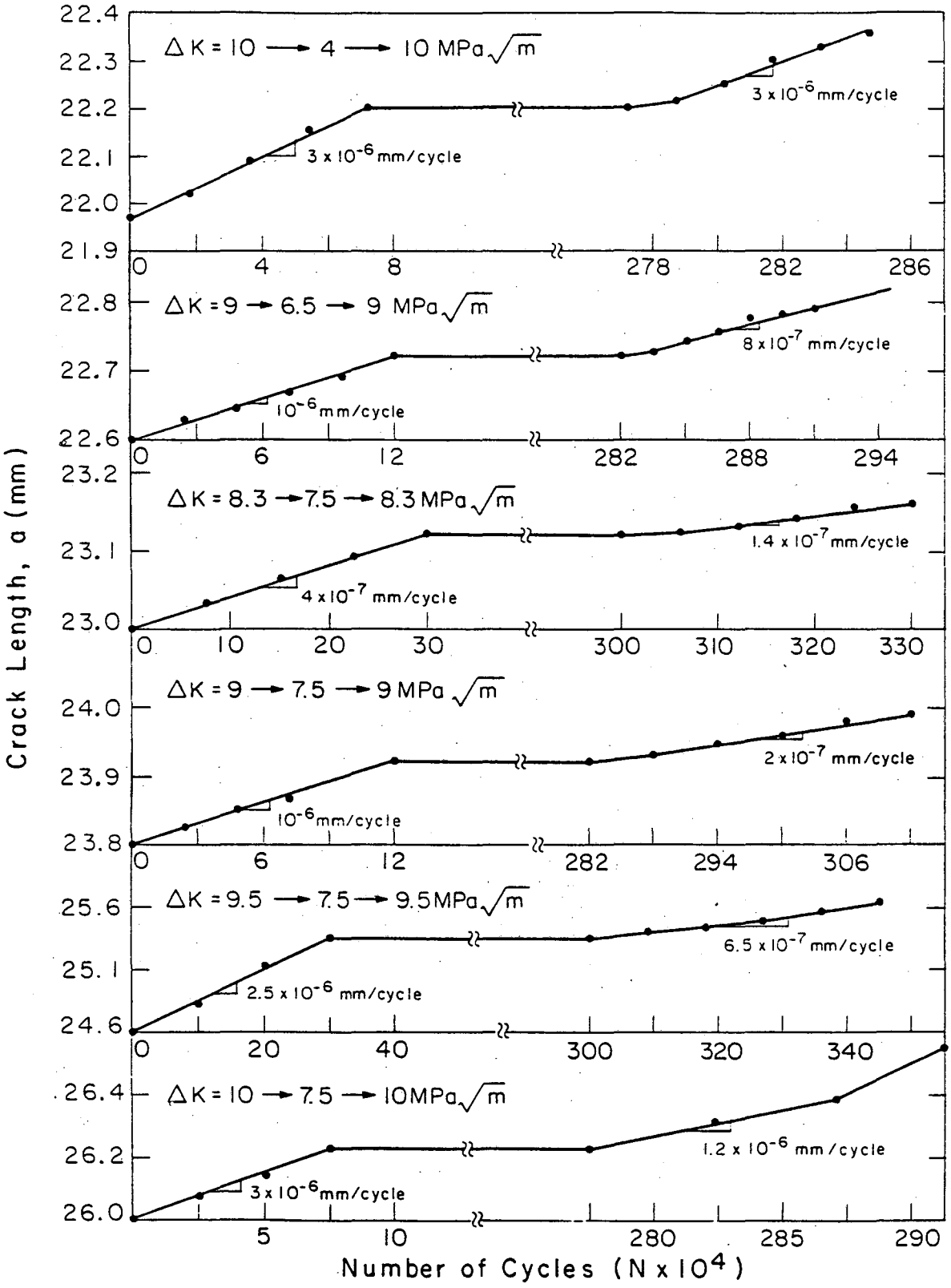

Figure 4

Crack length (a) versus number of cycles (N) data for underload tests, showing behavior prior to and immediately following the underload.

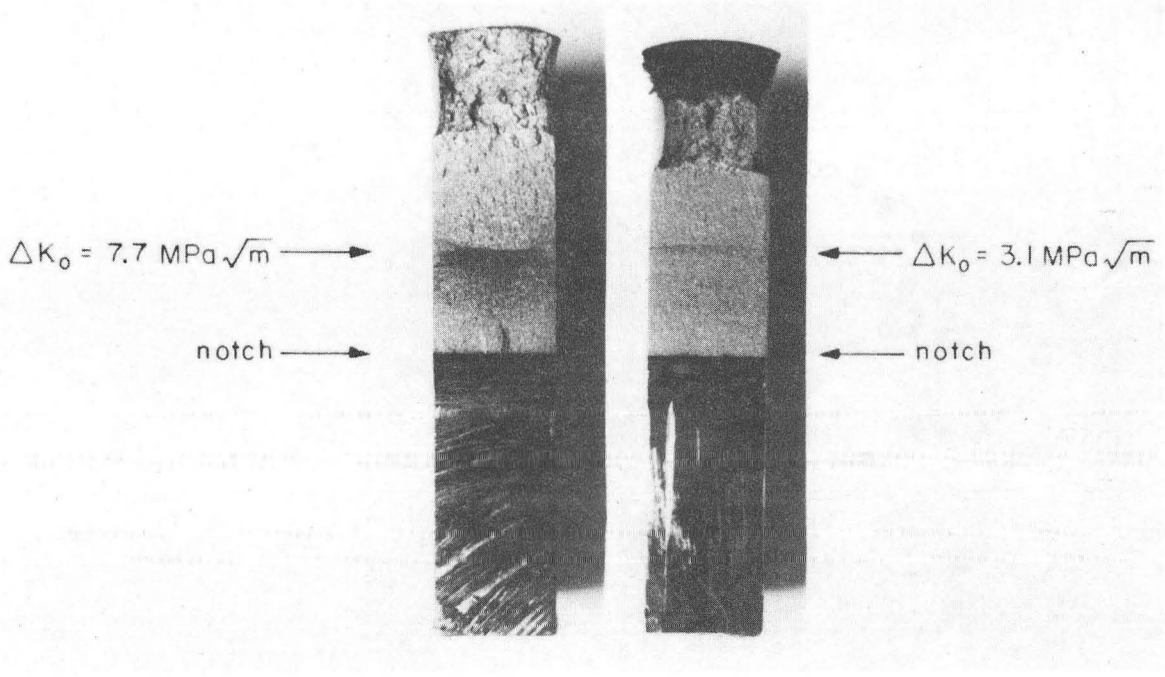

Figure 5

Bands of corrosion deposits visible on near-threshold fatigue fracture surfaces tested in moist air at R = 0.05 and 0.75.

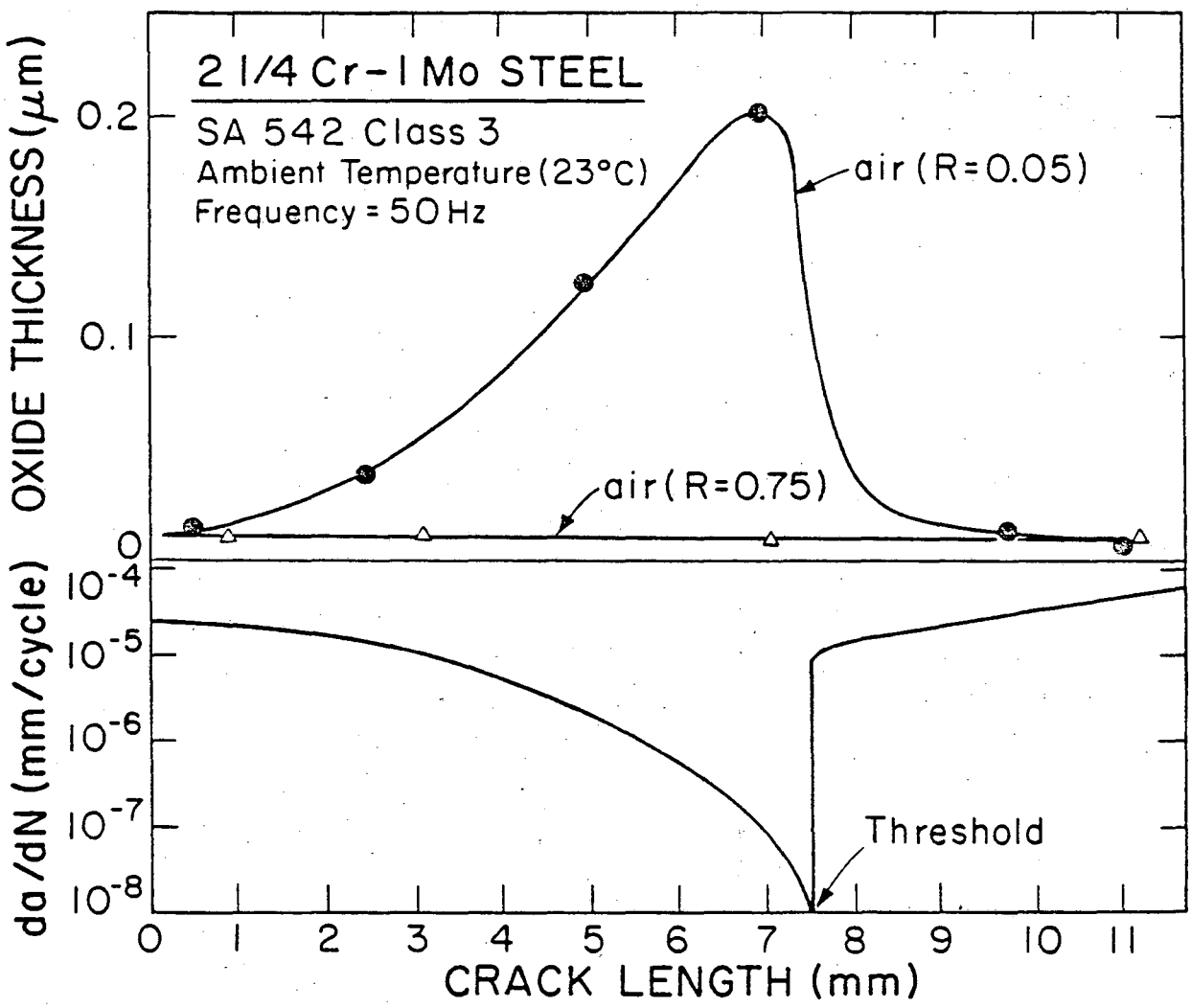

Figure 6

Measurement of crack flank oxide thickness (d) as a function of crack length (a) and crack growth rate (da/dN) for SA542-3 tested at R = 0.05 and 0.75 in moist air. Date from Ar^+ sputtering analysis using Auger spectroscopy.

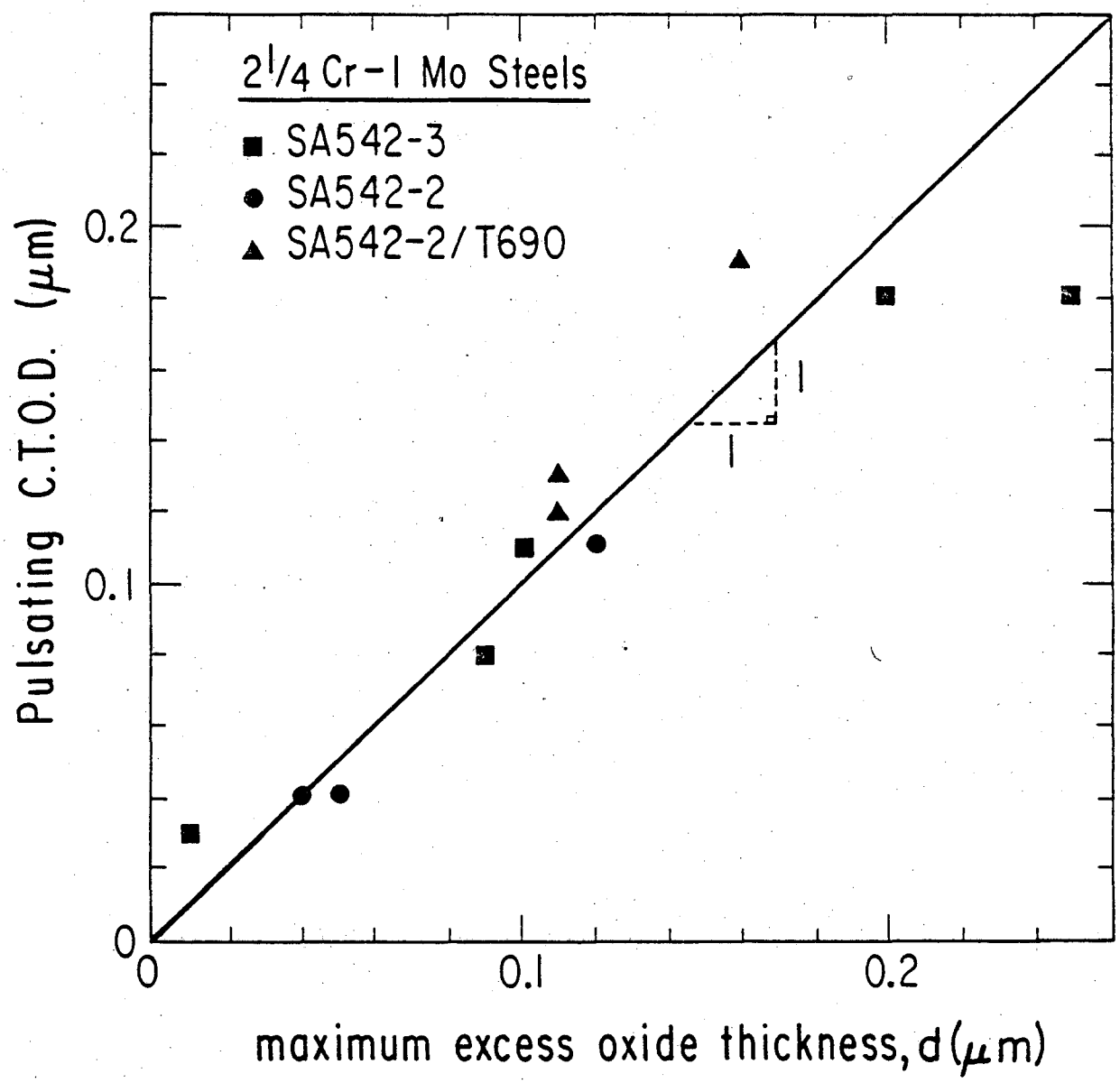

Figure 7

Correspondence of maximum excess oxide thickness with pulsating crack tip displacement (ΔCTOD) at the fatigue crack growth threshold ΔK_o, for a range of 2¼Cr-1Mo steels.

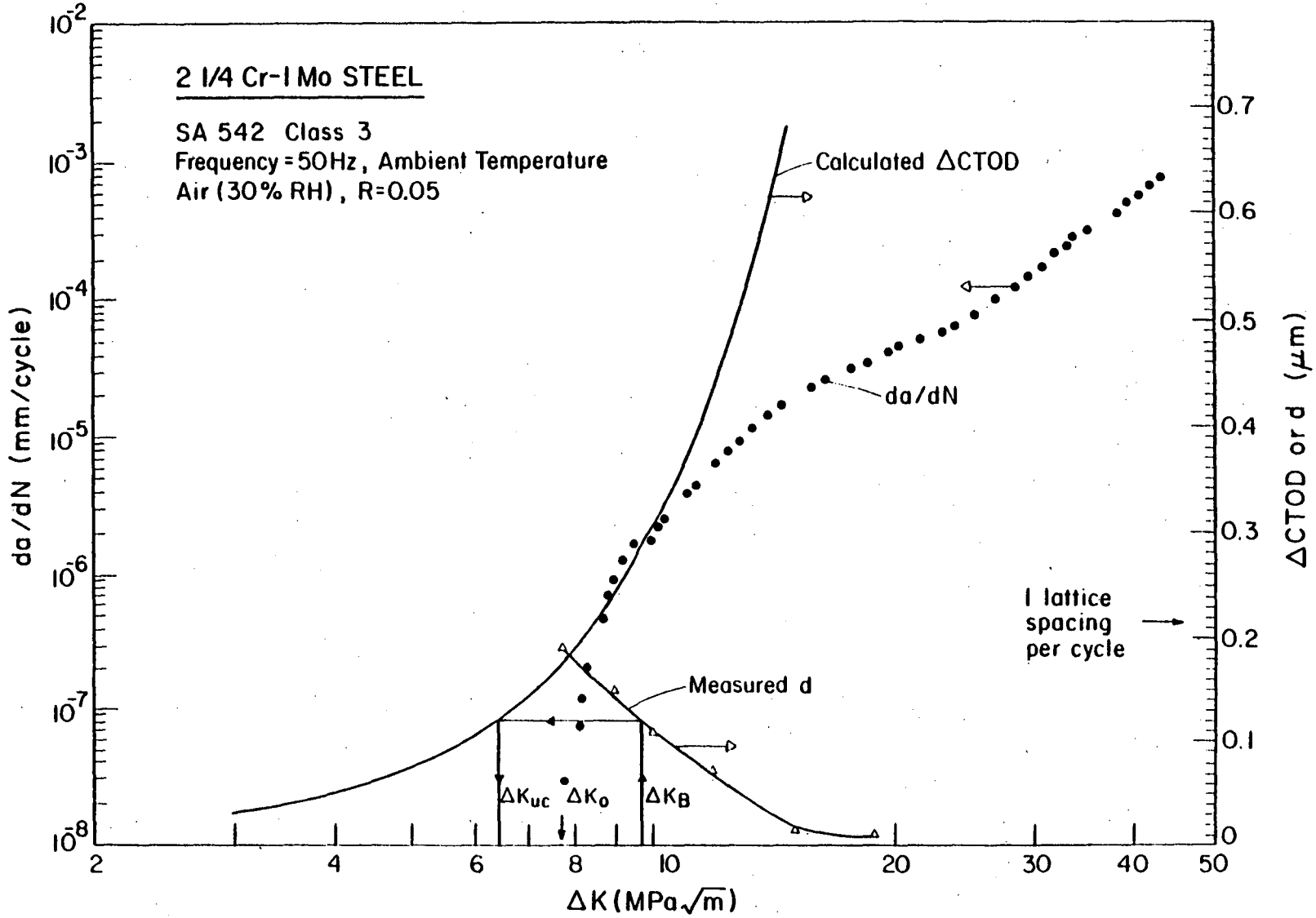

Figure 8

Crack growth rates (da/dN), measured excess oxide thickness (d), and computed pulsating crack tip displacements (ΔCTOD) as a function of ΔK for near-threshold fatigue behavior in SA542-3, showing potential influence of underload ΔK_u on baseline ΔK_B growth rates.

TECHNICAL INFORMATION DEPARTMENT
LAWRENCE BERKELEY LABORATORY
UNIVERSITY OF CALIFORNIA
BERKELEY, CALIFORNIA 94720